

Electronic structure of BAs and boride III–V alloys

Gus L. W. Hart and Alex Zunger

National Renewable Energy Laboratory, Golden, CO 80401

(Dated: October 24, 2018)

Boron arsenide, the typically-ignored member of the III–V arsenide series BAs–AlAs–GaAs–InAs is found to resemble silicon electronically: its Γ conduction band minimum is p -like (Γ_{15}), not s -like (Γ_{1c}), it has an X_{1c} -like indirect band gap, and its bond charge is distributed almost equally on the two atoms in the unit cell, exhibiting nearly perfect covalency. The reasons for these are tracked down to the anomalously low atomic p orbital energy in the boron and to the unusually strong s – s repulsion in BAs relative to most other III–V compounds. We find unexpected valence band offsets of BAs with respect to GaAs and AlAs. The valence band maximum (VBM) of BAs is significantly higher than that of AlAs, *despite* the much smaller bond length of BAs, and the VBM of GaAs is only slightly higher than in BAs. These effects result from the unusually strong mixing of the cation and anion states at the VBM. For the BAs–GaAs alloys, we find (i) a relatively small (~ 3.5 eV) and composition-independent band gap bowing. This means that while addition of small amounts of nitrogen to GaAs *lowers* the gap, addition of small amounts of boron to GaAs *raises* the gap (ii) boron “semi-localized” states in the conduction band (similar to those in GaN–GaAs alloys), and (iii) bulk mixing enthalpies which are smaller than in GaN–GaAs alloys. The unique features of boride III–V alloys offer new opportunities in band gap engineering.

I. INTRODUCTION

With the advent of state-of-the-art techniques for growing semiconductor alloys on common substrates such as GaAs, silicon, and germanium, semiconductor compounds which previously were very difficult to synthesize are now routinely achieved. Techniques such as metal-organic chemical vapor deposition (MOCVD), molecular beam epitaxy (MBE), and pulsed laser ablation (PLD) have provided the opportunity to synthesize and study a large number of nitride, phosphide, and antimonide semiconductor alloys. Of particular recent interest are alloys of a *wide gap* semiconductor (e.g. nitrides) with a “conventional” III–V semiconductor because of their promise in optical applications. Two diverging scenarios were considered: (i) using a significant amount (10%–30%) of the wide gap component to shift the alloy band gap to the *blue* (e.g., adding $\sim 20\%$ GaN to InN) for light-emitting diode or laser applications, and (ii) using a *small* amount of the wide gap semiconductor to shift the alloy band gap to the *red* (e.g., adding 1–3% GaN to GaAs) for photovoltaic applications. The latter effect occurs naturally if the band gap bowing parameter b is larger than the difference of the band gaps of the constituents (e.g., ZnS–ZnTe; GaAs–GaN). In this case addition of small amounts of the wide gap components acts to initially lower the band gap of the small gap component. For example, one can achieve the technologically desired 1 eV gap if one adds nitrogen to GaAs or to InGaAs.

When boron is substituted into GaAs, it can go to either a gallium site or an arsenic site. Normally boron

prefers isovalent substitution on the gallium site,^{1,2,3} which is the case we study here. In the other case when boron goes to the arsenic site (a boron “antisite” defect), the boron acts as an acceptor and this antisite defect has been the subject of numerous studies.^{4,5,6,7,8} Growth conditions determine whether boron goes to the gallium site as an isovalent substitution or to the arsenic site as an acceptor. For example, B_{As} antisite defects are known to occur in Ga-rich samples of GaAs grown by the liquid encapsulated Czochralski (LEC) method, but for GaAs crystals taken from stoichiometric or As-rich melts, electrically active boron or boron complexes are not found,⁹ indicating that the boron atoms have substituted isovalently to the gallium sites. Not as much is known about the *epitaxial* growth conditions under which isovalent or antisite boron incorporation occurs. It is reasonable to suppose that B_{As} antisite defects will be more likely under Ga-rich conditions and that As-rich growth conditions will lead to isovalent boron incorporation, similar to the case for LEC-grown GaAs. In this study, we focus on isovalent BGaAs alloys where boron occupies gallium sites.

In this paper we will explore BAs as an alternative to GaN as a wide gap partner for alloying conventional III–Vs such as AlAs and GaAs. Very little is known about BAs: As early as 1966, Ku mentioned the possibilities of BAs–GaAs as a boride III–V alloy with potentially useful properties.^{10,11} However, difficulties in fabricating BAs or simple solid solutions of zinc-blende BAs–GaAs^{10,12,13,14,15} prior to the development of current epitaxial techniques have prevented a careful study

of the alloy properties. Now that epitaxial techniques have eased these difficulties somewhat, boride semiconductor alloys are generating renewed interest.^{7,8,16,17,18} There are a number of theoretical studies that examine different aspects of pure BAs^{19,20,21,22,23,24,25,26} but theoretical studies of the boron *alloys* are lacking.

Important questions that one would want to answer include:

(i) How will alloying with BAs affect the band gaps and other properties of GaAs or AlAs?

(ii) To what extent does BAs fit the well-known trends in band gaps, band offsets and bonding patterns of the arsenide III–V series BAs–AlAs–GaAs–InAs?

(iii) Will the band gap bowing of $B_xGa_{1-x}As$ alloys be as anomalous as the (very large and composition-dependent) bowing in $GaAs_{1-x}N_x$?

(iv) Will cation substitution by boron lead to unusual wavefunction localization effects found to exist for anion substitution by nitrogen?^{27,28,29}

Two features of boron make boride semiconductors fundamentally different from common III–V or II–VI semiconductors. The first is that, like nitrogen, boron is in the first row of the periodic table and has deep p orbitals and a small atomic size. The second feature is, unlike nitrogen, boron has a low electronegativity. This leads to highly covalent compounds, unlike nitride semiconductors, which have a strong ionic character. This paper examines (i) zinc-blend BAs and its place in the III–As family of semiconductors and (ii) boron substitution of gallium in GaAs, including alloy bowing, band offsets and mixing enthalpies. Our main findings are:

Zinc-blende BAs: Surprisingly, we find that, electronically, BAs resembles silicon rather than other III–V semiconductors. Similar to silicon and in contrast to most III–Vs, the lowest Brillouin-zone center conduction band of BAs has p symmetry (Γ_{15c}) rather than s symmetry (Γ_{1c}), and, like silicon, its total valence charge density shows almost symmetric distribution of charge around the two atoms in the unit cell. The reasons for the silicon-like conduction band ordering in BAs are: (i) the small repulsion of the bonding and antibonding p states due to the low p orbital energy of boron, as well as the unusual hybridization of both cation and anion p states at the VBM, and (ii) the repulsion of the cation and anion s states which is much stronger in BAs than in AlAs, GaAs, and InAs. As a result of the p – p hybridization (covalent bonding) mentioned in (i), we also find that the valence band offset of BAs relative to other members of the III–As family is unusually high.

BAs–GaAs alloys: (i) The band gap bowing is relatively small (~ 3.5 eV) and composition-independent, in stark contrast to GaN–GaAs alloys. Because of this small bowing, the addition of BAs to GaAs *increases* the gap, thus, unlike nitrogen, addition of boron into GaAs or InGaAs will not lead to the desired 1 eV material. (ii) The lower energy conduction band states are “semi-localized” states around the boron atoms, e.g., the CBM is strongly localized near the boron but extended at longer distances

while the VBM is completely delocalized. (iii) The bulk mixing enthalpy of BAs in GaAs is much lower than that of GaN in GaAs, indicating that the bulk solubility of boron in III–V compounds may be higher than that of nitrogen and thus higher composition ranges may be possible with the boride alloys. These findings indicate that boride III–V alloys provide new opportunities in band gap engineering.

II. METHODS OF CALCULATION

A The LAPW calculations

We used density functional theory within the local density approximation (LDA),³⁰ as implemented by the full-potential linearized-augmented-planewaves (LAPW) method^{31,32} (WIEN97 implementation³³). The exchange-correlation potential of Perdew and Wang was used.³⁴ In the calculations with less than 32 atoms, the plane wave kinetic energy cutoff for the expansion in the interstitial region was 16 Ryd (approximately 130 basis function per atom). The muffin tin (MT) radii were 1.65 bohr for boron and 2.2 bohr for arsenic, aluminum, gallium, and indium. In the large supercell calculations (32 or more atoms), a slightly smaller plane wave kinetic energy cutoff 13 Ryd (approximately 120 basis functions per atom) and a larger boron MT radius of 1.8 bohr (2.1 for arsenic, aluminum, gallium, and indium) was used to ease the computational burden of the larger cells. Our convergence studies indicate that the error in the individual eigenstates is less than 5 meV for the valence and lower conduction bands. The calculations were run until the variation in the total energy between several self-consistency cycles was $< 10^{-5}$ Ryd. The experimental lattice constants were used in all the calculations of the individual compounds. The experimental lattice constants are 4.777 Å, 5.660 Å, 5.653, and 6.058 Å for BAs, AlAs, GaAs, and InAs, respectively.

The k point mesh used in the calculation of the simple binary compounds (zinc-blende BAs, AlAs, GaAs, and InAs) was a $4 \times 4 \times 4$ mesh of Monkhorst and Pack special points (10 points in the irreducible wedge of the Brillouin zone [BZ]).³⁵ The superlattice calculations for the valence band offsets as well as the supercell calculations for the alloy studies used k point meshes equivalent³⁶ to the $4 \times 4 \times 4$ mesh used in the calculation of the simple zinc-blende binary compounds. Using equivalent k point meshes is particularly important for calculations such as enthalpies of formation in order to eliminate uncertainties due to the statistical errors of different k point meshes. Thus, one can use much smaller k point meshes to achieve the required accuracies than would otherwise be necessary.

B Partial DOS, band characters, and valence charge density

It is useful to analyze the orbital character of different states. The band character (or orbital population) $Q_\ell^{(\alpha)}(\epsilon, \mathbf{k})$ is the ℓ -th angular momentum component of the charge due to wavefunction $\psi(\epsilon, \mathbf{k})$ enclosed in a sphere Ω_{MT} of radius $R_{MT}^{(\alpha)}$ about atom α

$$Q_\ell^{(\alpha)}(\epsilon, \mathbf{k}) = \int_{\Omega_{MT}} |\hat{P}_\ell \psi(\epsilon, \mathbf{k}, \mathbf{r})|^2 d\mathbf{r} \quad (1)$$

where \hat{P}_ℓ is an angular momentum projection operator with origin at site α . Because the interstitial region outside the muffin tin spheres is excluded when the band characters are calculated, the muffin tin radii were chosen to match the rationalized tetrahedral radii of Phillips.³⁷

The partial DOS are determined by integrating $Q_\ell^{(\alpha)}(\epsilon, \mathbf{k})$ over all \mathbf{k} in the Brillouin zone (BZ);

$$N_\ell^{(\alpha)}(\epsilon) = \int_{BZ} Q_\ell^{(\alpha)}(\epsilon, \mathbf{k}) d\mathbf{k}. \quad (2)$$

The angular-momentum decomposition of the total valence charge can then be determined by summing $N_\ell(\epsilon)$ over the valence bands;

$$q_\ell^{\text{tot}} = \int_{V_{B\text{min}}}^{V_{B\text{max}}} N_\ell(\epsilon) d\epsilon. \quad (3)$$

Valence charge densities: The charge density is constructed from the highest N_B occupied bands as

$$\rho_{\text{val}}(\mathbf{r}) = \sum_{n=1}^{N_B} \int_{BZ} |\psi_{n,\mathbf{k}}(\mathbf{r})|^2 d\mathbf{k}. \quad (4)$$

For plotting ρ_{val} we use $N_B = 4$. Thus, cation d bands are not included in the construction.

The ‘‘valence deformation density’’ $\Delta\rho_{\text{val}}(\mathbf{r})$ describes the difference between the solid-state density and a superposition of densities of spherical atoms in their ground state,

$$\Delta\rho_{\text{val}}(\mathbf{r}) = \rho_{\text{val}}(\mathbf{r}) - \rho_{\text{sup}}(\mathbf{r}). \quad (5)$$

The valence charge difference is defined as the difference between the crystal valence density (including the cation d bands, when occupied) and a superposition of free, spherical LDA atomic densities arranged in the configuration of the crystal. The atomic configuration of the free atoms are $d^{10}s^2p^1$ for the cations and s^2p^3 for the anions.

C Band offsets

The offset $\Delta E_v(\text{AX}/\text{BY})$ between the valence band maxima of two semiconductor compounds AX and BY

TABLE I: Convergence test for the valence band offsets of BAs/GaAs, BAs/AlAs, and AlAs/GaAs using two different superlattice periods. Units are eV. Band offsets were calculated using both anion and cation core states [see Eq. (6)]. Note that while for AlAs/GaAs a similar offset is obtained when either anion or cation core levels are used, for the borides only anion core levels provide a rapidly convergent band offset with respect to the superlattice period n .

Superlattice	Using 1s anion	Using 2s anion	Using 1s cation
(BAs) ₂ /(GaAs) ₂	0.18	0.11	0.83
(BAs) ₄ /(GaAs) ₄	0.19	0.12	0.58
(BAs) ₂ /(AlAs) ₂	-0.38	-0.45	0.58
(BAs) ₄ /(AlAs) ₄	-0.39	-0.47	0.17
(AlAs) ₂ /(GaAs) ₂	0.50	0.50	0.41
(AlAs) ₄ /(GaAs) ₄	0.51	0.51	0.47

forming a heterostructure is calculated using a method similar to that used in photoemission spectroscopy.³⁸

$$E_v(\text{AX}/\text{BY}) = \Delta E_{v,C'}^{BY} - \Delta E_{v,C}^{AX} + \Delta E_{C,C'}^{AX/BY}, \quad (6)$$

where

$$\begin{aligned} \Delta E_{v,C}^{AX} &= E_v^{AX} - E_C^{AX} \\ \Delta E_{v,C'}^{BY} &= E_v^{BY} - E_{C'}^{BY} \end{aligned} \quad (7)$$

are the energy separations between the core levels (C and C') and the valence band maximums for the pure AX and BY compounds. The third term in equation (6),

$$\Delta E_{C,C'}^{AX/BY} = E_{C'}^{BY} - E_C^{AX} \quad (8)$$

is the difference in the core level binding energy between the two compounds AX and BY in the AX/BY heterojunction. To calculate the ‘‘natural band offset’’, $\Delta E_{v,C}^{AX}$ and $\Delta E_{v,C'}^{BY}$ are calculated for AX and BY at their cubic, equilibrium lattice constants. The core level difference $\Delta E_{C,C'}^{AX/BY}$ is obtained from calculations of $(\text{AX})_n/(\text{BY})_n$ superlattices in the (001) direction. The period n needs to be large enough so that AX -like and BY -like properties can be identified far from the interface. For the core states (denoted C and C'), we use the anion 1s states. Table I shows the dependence of the valence band offset calculations on the period of the superlattice and on which core states are used. Because of the large size mismatch of BAs and GaAs, at least $n = 4$ is required to sufficiently converge $\Delta E_{C,C'}^{AX/BY}$. We also find that while a similar offset is obtained for AlAs/GaAs when either anion or cation core levels are used, for the borides only anion core levels provide a rapidly convergent band offset with respect to the superlattice period n .

TABLE II: Definition of the supercells used in this study and equivalent k points. Lattice vectors are given in units of a_0 and equivalent k points are given as fractions of the reciprocal lattice vectors.

System	Lattice vectors	Equivalent k points	Relative weight
AC, BC zinc-blende	$(1/2, 1/2, 0)$ $(1/2, 0, 1/2)$ $(0, 1/2, 1/2)$	$(0, 0, 1/8)$	1
		$(0, 0, 3/8)$	1
		$(0, 1/8, 3/4)$	3
		$(0, 1/8, 1/4)$	3
		$(0, 1/8, 1/2)$	3
		$(0, 1/4, 5/8)$	3
		$(1/8, 1/4, 1/2)$	6
		$(0, 1/4, 3/8)$	3
		$(0, 3/8, 1/2)$	3
		$(1/8, 3/8, 5/8)$	6
		$(AC)_1/(BC)_1$ (100) superlattice	$(1/2, 1/2, 0)$ $(1/2, -1/2, 0)$ $(0, 0, 1)$
$(0, 1/8, 3/8)$	1		
$(0, 3/8, 1/8)$	1		
$(0, 3/8, 3/8)$	1		
$(1/8, 1/4, 1/8)$	2		
$(1/8, 1/4, 3/8)$	2		
$(1/8, 1/2, 1/8)$	1		
$(1/8, 1/2, 3/8)$	1		
$(1/4, 3/8, 1/8)$	2		
$(1/4, 3/8, 3/8)$	2		
$(3/8, 1/2, 1/8)$	1		
$(3/8, 1/2, 3/8)$	1		
$(AC)_2/(BC)_2$ (100) superlattice	$(1/2, 1/2, 0)$ $(1/2, -1/2, 0)$ $(0, 0, 2)$		
		$(0, 3/8, 1/4)$	1
		$(1/8, 1/4, 1/4)$	2
		$(1/8, 1/2, 1/4)$	1
		$(1/4, 3/8, 1/4)$	2
		$(3/8, 1/2, 1/4)$	1
$(AC)_4/(BC)_4$ (100) superlattice	$(1/2, 1/2, 0)$ $(1/2, -1/2, 0)$ $(0, 0, 4)$	$(0, 1/8, 1/2)$	1
		$(0, 3/8, 1/2)$	1
		$(1/8, 1/4, 1/2)$	2
		$(1/8, 1/2, 1/2)$	1
		$(1/4, 3/8, 1/2)$	2
		$(3/8, 1/2, 1/2)$	1
$A_1B_7C_8$ fcc supercell	$(1, 1, 0)$ $(1, 0, 1)$ $(0, 1, 1)$	$(0, 0, 1/4)$	1
		$(0, 1/4, 1/2)$	3
$A_1B_{15}C_{16}$ bcc supercell	$(1, 1, -1)$ $(1, -1, 1)$ $(-1, 1, 1)$	$(1/8, 1/8, 1/8)$	1
		$(1/8, 5/8, 5/8)$	1
$A_1B_{31}C_{32}$ simple cubic supercell	$(2, 0, 0)$ $(0, 2, 0)$ $(0, 0, 2)$	$(1/4, 1/4, 1/4)$	1
$A_8B_8C_{16}$ SQS16	$(1, -1, 2)$ $(1, -1, -2)$ $(1/2, 1/2, 0)$	$(0, 1/2, 0)$	1
		$(1/2, 0, 0)$	1
		$(1/4, 3/4, 1/8)$	4
		$(0, 1/2, 1/4)$	2
		$(1/2, 0, 1/4)$	2
		$(1/4, 3/4, 3/8)$	4
		$(0, 1/2, 1/2)$	1
$(1/2, 0, 1/2)$	1		

D Alloy enthalpies of mixing, alloy bowing, and equivalent k points

The *enthalpy of mixing* for an alloy $A_{1-x}B_x$ of two components A and B is the difference in energy between the alloy and the weighted sum of the constituents;

$$\Delta H(x) = E_{A_pB_q} - [(1-x)E_A + xE_B] \quad (9)$$

where $x = p/(p+q)$. In the mixing enthalpy calculations, the alloy lattice constant $a(x)$ is taken as the linear average of the experimental values of the constituents. The experimental lattice constants of BAs and GaAs are 4.777 Å and 5.653 Å, respectively, whereas the calculated lattice constants are 4.740 Å and 5.615 Å. Any free internal coordinates in the alloy structure were relaxed using the

quantum mechanical forces so that residual forces on the ions were less than 1 mRyd/bohr.

The *band gap bowing* parameter b defined by

$$E_g(x) = \overline{E}_g(x) - bx(x-1), \quad (10)$$

where $\overline{E}_g(x)$ is the weighted linear average of the individual band gaps of A and B . The bowing parameter b represents the deviation of the band gap from this average. Note that although there are LDA errors in the calculated gaps of the A_xB_{1-x} alloy as well as the pure constituents A and B , to lowest order, the LDA error in the bowing b cancels out.

Considering Eqs. (9) and (10), we see that one needs to converge the k representation for a compound A_pB_q as well as for the elemental constituents A and B . The stan-

TABLE III: All possible pair configurations in the 64 atom cell.

Shell number (n th fcc neighbor)	Lattice vector $[u, v, w]$ (unit $a_0/2$)	Number of equivalent pairs
1	[0, 1, 1]	12
2	[2, 0, 0]	3
3	[2, 1, 1]	12
4	[2, 2, 0]	3
6	[2, 2, 2]	1

standard way of accomplishing this is to increase the number of k points in all three systems until convergence is obtained. The disadvantage of this approach is that it requires *absolute* k point convergence for A and B , and separately for $A_p B_q$. A better approach is to take advantage of *relative* k point convergence.³⁶ The idea is to sample the Brillouin zone *equivalently* for A , B and $A_p B_q$. This could be done by considering $A_p A_q$, $B_p B_q$, and $A_p B_q$ as isostructural solids and sampling the Brillouin zone of each equally. Then, any relative k -point sampling error cancels out. This is called the *method of equivalent k points*.³⁶ In practice, one does not have to calculate $A_p A_q$ and $B_p B_q$ but instead can calculate A and B in their primitive unit cells using suitably folded-in k points. Equivalent k points for the unit cells in this paper are given Table II.

E Choice of supercells

The calculations of ΔH [Eq. (9)] and b [Eq. (10)] require supercells. We use $B_1Ga_7As_8$, $B_1Ga_{15}As_{16}$, $B_1Ga_{31}As_{32}$, and $B_2Ga_{30}As_{32}$. The lattice vectors defining the supercells are given in Table II. The SQS16 supercell is a “special quasirandom structure”—a periodic structure with rather small unit cell whose lattice sites are occupied by A and B atoms so as to mimic the atom-atom correlation functions of much larger $A_{1-x}B_x$ supercells with random occupations.³⁹

In the calculations for the band gap bowing of $B_xGa_{1-x}As$ alloys, 64 atom, simple-cubic unit cells were used for both the 3% and 6% boron alloys. In the case of the 3% alloy, there is one boron atom in the supercell, but for the 6% alloy, there are two boron atoms in the supercell. For this case, the band gap was determined by taking the weighted average of the gaps for the 5 symmetrically-inequivalent configurations (given in Table III) of two boron atoms in the 64 atom supercell. These 5 pairs are the first through fourth neighbor pairs in an fcc lattice, as well as the sixth neighbor. (In the 64 atom cell, the fifth fcc neighbor is equivalent to the first.) Using the same 64 atom unit cell for the alloys in the bowing calculations eliminated band gap differences that can occur due to the k -point folding relations of different supercells, as discussed by Bellaiche et al. in Ref. 28.

TABLE IV: Parameters used in the VFF model. d_{bond}^0 is the equilibrium (unstretched) bond length, α is the bond stretch term, β is the bond bending term, and σ is the stretching-bending term. The units of α , β , and σ are 10^3 dyne.

System	$d_{\text{bond}}^0(\text{\AA})$	α	β	σ
For band gap bowing				
BAs	2.0685	76.26	19.12	-9.12
GaAs	2.4480	32.15	9.37	-4.10
For mixing enthalpy				
BAs	2.0685	76.26	22.2	—
GaAs	2.4480	41.19	8.94	—
GaN	1.9520	96.30	14.8	—

F Valence force field model

In two cases, the total energies or the internal structural parameters were determined using a classical force field model. This generalized valence force field model^{40,41} (VFF) consists of bond stretching, bond bending, and bending-stretching springs with force constants σ , β , and σ , respectively. The force constants and the equilibrium (no force) bond lengths are given in Table IV. The two cases where the VFF model was used are:

(1) The VFF model was used to model the mixing enthalpies of boron or nitrogen in GaAs in the regime of very low concentrations (Sec. V C). Because well tested force constants exist for the “conventional” VFF model (α , β ; no σ) for the case of GaAs/GaN, we also used a two-parameter ($\sigma = 0$) model for BAs/GaAs for the sake of consistency with previous calculations. The parameters for BAs/GaAs were tested by comparing the enthalpies of formation for structures at higher concentrations calculated using first principles, as given in Table V.

(2) Full relaxation using first principles’ forces of all 64 atom supercells used in the band gap bowing calculations reported in Sec. V B is computationally prohibitive so the generalized⁴¹ VFF model was used to determine internal coordinates. In one case ($B_1Ga_{31}As_{32}$), the VFF- and LAPW-determined coordinates were compared and found to be very similar. The average difference between the two methods for the Ga-As bonds was $< .005$ a.u. (0.1%). The largest discrepancy was near the boron site where the VFF predicts a B-As bond length that is 0.01 a.u. (1.5%) shorter than the LAPW bond length. Using the VFF-determined internal coordinates of the supercell would be acceptably accurate only if the band gap is very close to that when the first-principles’ coordinates are used. In the case of the $BGa_{31}As_{32}$ supercell just mentioned, the band gap difference was only 10 meV, justifying the use of the VFF.

TABLE V: Enthalpies of formation (LDA and VFF) of ordered (001) superlattices of BAs/GaAs and the mixing enthalpies of $B_xGa_{1-x}As$ random alloys [Eq. (9)]. All the ΔH values are positive.

System	Boron concentration	ΔH (meV/atom) (LAPW)	ΔH (meV/atom) (VFF)
Ordered superlattices:			
$(BAs)_1/(GaAs)_1$ (001)	50%	186	193
$(BAs)_2/(GaAs)_2$ (001)	50%	171	192
$(BAs)_4/(GaAs)_4$ (001)	50%	161	191
$(BAs)_\infty/(GaAs)_\infty$ (001)	50%	148	—
$(BAs)_1/(GaAs)_3$ (001)	25%	132	174
Random alloys:			
BGa_7As_8 (fcc)	12.5%	73	79
$BGa_{15}As_{16}$ (bcc)	6.25%	22	30
$BGa_{31}As_{32}$ (simple cubic)	3.13%	9.5	16

III. BAs AND THE III-As FAMILY

A. Expectations from atomic physics

The LDA valence orbital energies for the first four elements of column III are plotted in Fig. 1. The lower value of the atomic p states of B relative to the atomic p states for Al, Ga, and In (which are all quite similar) are notable. This lower value can be understood from the fact that, as a first row element, the $2p$ states in B need not be orthogonal to lower p states. In general, the cation s energy should increase going down the column

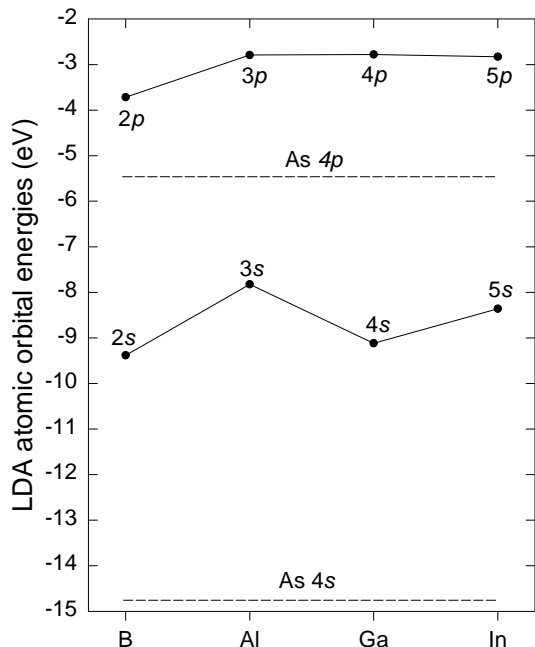


FIG. 1: Atomic s and p orbital energies in column III of the Periodic Table. Calculated fully relativistically within the local density approximation.

but there is a kink when moving from Al to Ga due to the introduction of imperfectly screened d states in Ga. The fact that the p states in B lie lower in energy, and hence closer to the As $4p$ states, will lead to a much stronger hybridization of p -like states in BAs relative to the other III-As systems.

The consequence of this is shown in Fig. 2 which shows the total valence charge, q_ℓ^{tot} of angular momentum ℓ [Eq. (3)], enclosed in spheres having the tetrahedral radii of Phillips.³⁷ It is clear that the occupation of the B and As p -like states in BAs is much higher than in the other systems (indicating that p - p hybridization is much more pronounced in BAs) and also that there is more charge

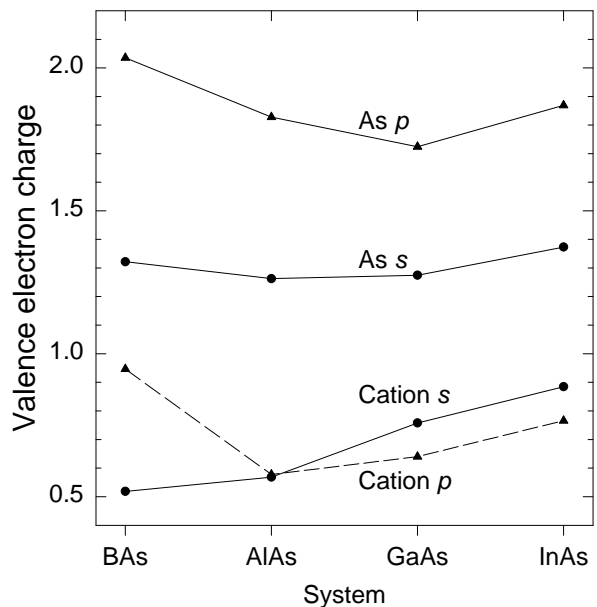


FIG. 2: Total valence charge [Eq. (4)] enclosed in spheres having the tetrahedral radii of Phillips:³⁷ boron 0.853 Å, aluminum 1.230 Å, gallium and arsenic 1.225 Å, and indium 1.405 Å.

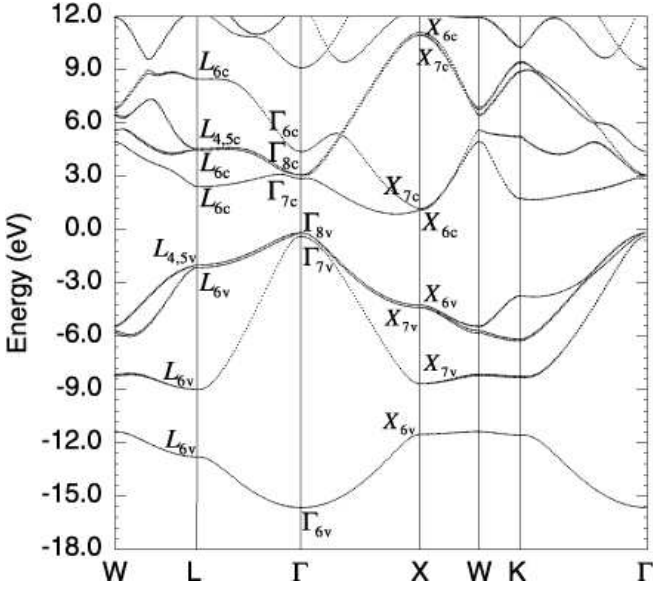


FIG. 3: Relativistic energy band structure of BAs. The VBM is taken to be zero and the lattice constant is 4.777 Å.

around the boron than the other cations. Thus, the distinction between “cation” and “anion” is not so clear cut in BAs, where both atoms share similar charge. This is also reflected in the relative ionicities in the group. According to the Phillips scale⁴² the relative ionicities are .002, .274, .310, and .357 for BAs, AlAs, GaAs, and InAs, respectively. As a result of the relative ionicities, the bonding in BAs is almost completely covalent whereas the other three members of the group have a significant ionic component that increases in the order AlAs → GaAs → InAs. We will see next how these expectations are reflected in the electronic structure of BAs.

B Energy bands, band characters, and densities of states in zinc-blende BAs

The energy bands of zinc-blende BAs are shown in Fig. 3. Calculated band energies at high symmetry points are given in Table VI.^{24,34} As others have shown previously,^{13,19,23,24} the band gap of BAs is indirect; the CBM is along the Δ line between the Γ and X points— at approximately $0.82(1, 0, 0)2\pi/a$. An unusual feature of the band structure is the character of the CBM at Γ . In BAs, the CBM is the p -like Γ_{7c} state (Γ_{15c} if spin-orbit interaction not included). Only the semiconductors silicon and BP share this feature. In most semiconductors, the lowest state at Γ is the singly degenerate s -like state. The origins of this feature of the BAs band structure can be understood in the context of the tight-binding model of Harrison.⁴³ According to this model, the bonding (Γ_{15v})

TABLE VI: Comparison of BAs band energies for LDA and GW.²⁴ Two LDA values are given: all-electron LAPW values from this work and pseudopotential plane-wave (PP) values.²⁴ All the calculations used the experimental lattice constant of 4.777 Å. The exchange-correlation potential used in the PP calculations was not reported. For our LAPW calculations, the exchange-correlation of Perdew and Wang³⁴ was used (See Sec. II for details.)

	LDA-PP (eV)	LDA-LAPW (eV)	GW (eV)
Γ_{6c}	4.5	4.57	5.5
Γ_{8c} ($\times 2$)	3.3	3.26	4.2
Γ_{7c}	3.1	3.05	4.0
Γ_{8v} ($\times 2$)	0.00	0.00	0.00
Γ_{7v}	-0.22	-0.21	-0.22
Γ_{6v}	-15.5	-15.46	-16.7
X_{6c}	11.4	11.27	13.1
X_{7c}	11.2	11.13	12.9
X_{6c}	1.38	1.274	1.86
X_{7c}	1.36	1.359	1.93
X_{6v}	-4.1	-4.07	-4.5
X_{7v}	-4.2	-4.21	-4.6
X_{7v}	-8.6	-8.49	-9.5
X_{6v}	-11.3	-11.35	-12.2
L_{6c}	8.8	8.65	9.8
$L_{4,5c}$	4.8	4.74	5.7
L_{6c}	4.7	4.66	5.6
L_{6c}	2.6	2.60	3.3
$L_{4,5v}$	-1.8	-1.81	-2.0
L_{6v}	-1.9	-1.96	-2.1
L_{6v}	-8.8	-8.82	-9.7
L_{6v}	-12.6	-12.62	-13.6

and antibonding (Γ_{15c}) p states at Γ are given by

$$E(\Gamma_{15}) = \frac{\varepsilon_p^c + \varepsilon_p^a}{2} \pm \sqrt{\left(\frac{\varepsilon_p^c - \varepsilon_p^a}{2}\right)^2 + (4E_{pp})^2} \quad (11)$$

where ε_p^c and ε_p^a are the p atomic orbital energies for the cation (c) and the anion (a) and the interatomic term E_{pp} is proportional to $1/d_{\text{bond}}^2$ where d_{bond} is the bond length. The bonding (Γ_{1v}) and antibonding (Γ_{1c}) s states at Γ are given by

$$E(\Gamma_1) = \frac{\varepsilon_s^c + \varepsilon_s^a}{2} \pm \sqrt{\left(\frac{\varepsilon_s^c - \varepsilon_s^a}{2}\right)^2 + (4E_{ss})^2} \quad (12)$$

where ε_s^c and ε_s^a are the s atomic orbital energies for the cation (c) and the anion (a) and the interatomic term E_{ss} is again proportional to $1/d_{\text{bond}}^2$. A schematic diagram of the BAs energy levels in this model is shown in Fig. 4a.

The reversal of the conduction band states in the BAs band structure relative to other III–V compounds is a result of two effects: (i) a small Γ_{15v} – Γ_{15c} bonding/antibonding repulsion due to the small E_{pp} , as described by Eq. (11), and (ii) a large Γ_{1v} – Γ_{1c} repulsion of due to the small $(\varepsilon_s^B - \varepsilon_s^A)^2$, as described by

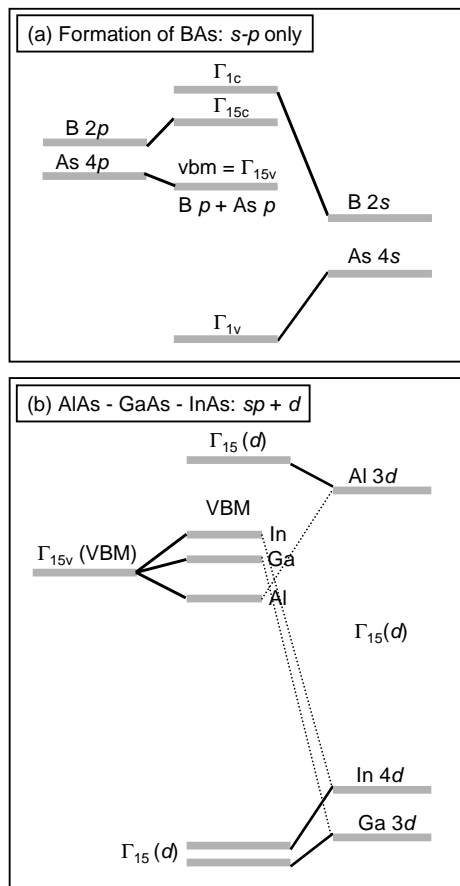


FIG. 4: Schematic diagram of energy levels in the III–As series. (a) Schematic diagram of energy levels in zincblende BAs and their atomic origins. Because the B- p -As- p orbital energy difference is small relative to other III–V compounds and the B- s -As- s orbital energy difference is large, the p -like Γ_{15c} conduction band state is *below* the s -like Γ_{1c} conduction band state. This ordering of the lower conduction band states is unusual for III–V compounds and is reminiscent of silicon. (b) Schematic diagram of the effects of p - d coupling on the VBM in AlAs, GaAs, and InAs. The VBM is driven up by the coupling of the $3d(4d)$ states in GaAs(InAs) and the As $4p$ -like VBM, but in AlAs, this p - d repulsion drives the VBM down.

Eq. (12). As is evident from Fig. 4, a small Γ_{15v} - Γ_{15c} bonding/antibonding repulsion will lower the Γ_{15c} state and a large Γ_{1v} - Γ_{1c} bonding/antibonding repulsion will raise the Γ_{1c} . In BAs these two effects are enough to reverse the ordering of the Γ_{15c} and Γ_{1c} states.

The large Γ_{1v} - Γ_{1c} bonding/antibonding difference is due to the large E_{ss} due to the short bond length in BAs. Empirical tight binding has also shown that the Γ_{1v} - Γ_{1c} repulsion is much more pronounced in BN, BP, and BAs than in other III–Vs.²³ The small Γ_{15v} - Γ_{15c} bonding/antibonding repulsion is due to the small differences in the p atomic orbitals of the boron and arsenic, as

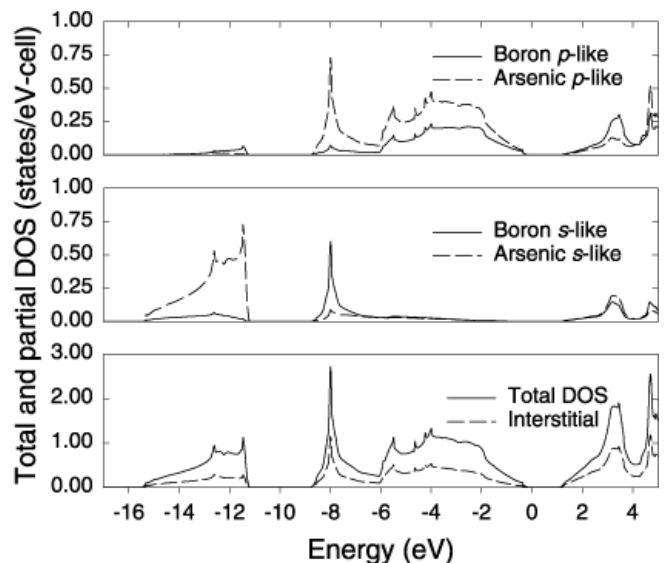


FIG. 5: Partial and total densities of states for BAs [Eq. (2)] inside muffin tin spheres with radii 0.853 Å for boron and 1.225 Å for arsenic.³⁷ Note the strong mixing of B and As p states. Figure 2 shows a quantitative measure of the p - p mixing in the each of the III–As compounds.

shown in Fig. 1. That is, the first term under the radical in Eq. (11) is small relative to other III–Vs.

The strong hybridization of the B and As p states is visible in the partial densities of states plot [Eq. (2)] in Fig. 5 and band character plots in Fig. 6 [Eq. (1)] where the width of the lines indicates the amount of the character indicated in the plot label. From these plots, one can see that the s band of arsenic between -12 and -16 eV is distinct and has very little mixing with other states. This is similar to the other three III–As systems, although in the case of BAs the arsenic s band is wider and somewhat lower in energy. Two unique features of the BAs DOS compared to other III–V semiconductors is the pronounced boron p character at the VBM and anion p character at the CBM. The stronger p - p hybridization in BAs relative to the rest of the III–As is due to the proximity of the orbital energies of B and As and the short bond length in the compound.

C Trends in band gap and inter-valley energy differences along the III-As family

Figure 7 shows the LDA-calculated vs. experimental band gaps for the III–As family, MAs (M = B, Al, Ga, In). For all but BAs, LDA energy band gaps are taken from the LAPW calculations reported in Ref. 44. Experimental band gaps are from Ref. 45 For BAs, for which no reliable experimental data exists, we used the GW band gap from Ref. 24. Because of the unusual ordering

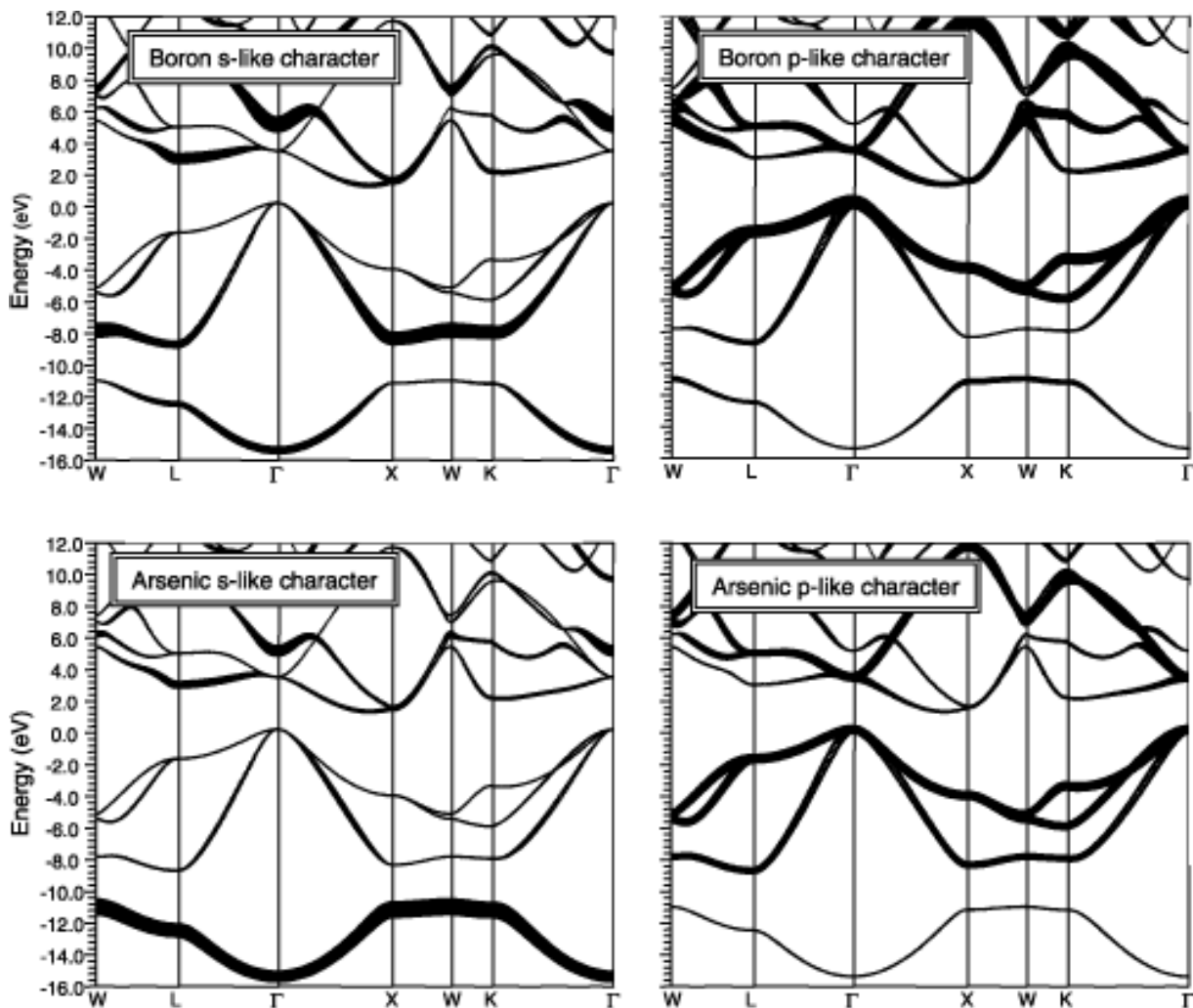


FIG. 6: Band characters of BAs [Eq. (1)] plotted as a function of k . The thickness of the lines denotes a relative amount of a given character. The B and As p states are strongly mixed at both the VBM and the CBM whereas the As s band is distinct. There is some mixing of As p and B s states in the bottom of the p - p hybridized bands.

of the conduction bands in BAs, the direct gap is not the $\Gamma_{15v} \rightarrow \Gamma_{1c}$ gap but the $\Gamma_{15v} \rightarrow \Gamma_{15c}$. The figures show the $\Gamma_{15v} \rightarrow \Gamma_{1c}$ gaps (which are the direct gaps in AlAs, GaAs, and InAs). We find in Fig. 7 that the LDA vs. expt. $\Gamma_{15v} \rightarrow \Gamma_{1c}$ and the $\Gamma_{15v} \rightarrow L_c$ gaps lie almost on a straight line. The LDA error of these gaps in the III-As family is approximately constant, even for BAs. For the $\Gamma_{15v} \rightarrow \Gamma_{1c}$ gaps, the magnitude of the error is ~ 1 – 1.5 eV. For the $\Gamma_{15v} \rightarrow L_c$ gaps, the magnitude of the error is ~ 0.7 – 1.1 eV. The experimental $\Gamma_{15v} \rightarrow X_c$ gaps only vary by ~ 0.5 eV through the series and corresponding LDA gaps are nearly identical, resulting in a tight clustering of the $\Gamma_{15v} \rightarrow X_c$ points in Fig. 7.

In Fig. 8(a), we show the $\Gamma_{15v} \rightarrow \Gamma_{1c}$, $\Gamma_{15v} \rightarrow L_c$, and $\Gamma_{15v} \rightarrow X_c$ gaps for the III-As family. We see: (i) the ordering of the conduction band states in BAs and AlAs is $X_{1c} < L_{1c} < \Gamma_{1c}$ whereas (ii) the ordering is $\Gamma_{1c} < L_{1c} < X_{1c}$ for GaAs and InAs, (iii) the X_{1c} and

L_{1c} states are closely spaced in AlAs and GaAs, (iv) BAs is “strongly indirect;” L_{1c} and Γ_{1c} are far above the CBM (which is close to X_{1c}), and (v) a crossing of the lowest X and L conduction states occurs between AlAs and GaAs, but the $\Gamma_{15v} \rightarrow \Gamma_{1c}$ gaps decrease so rapidly in the series that the Γ_{1c} states lie below the L_{1c} in GaAs and InAs, and thus these two members of the family are direct band gap materials (whereas BAs and AlAs are indirect X gap materials).

Figure 8(b) shows the conduction band intervalley differences $\Gamma_{1c} \rightarrow X_c$ and $\Gamma_{1c} \rightarrow L_{1c}$. Both differences show a smoothly decreasing trend from AlAs to GaAs to InAs, but an anomalously large decrease from BAs to AlAs. Again, this is a result of the enhanced s - s repulsion in BAs. Because the Γ_{1c} state has much more s character than either the lowest X and L conduction states (see Fig. 6), the effect of the s - s repulsion is greater for the Γ_{1c} than for these other two states, driving it up relative

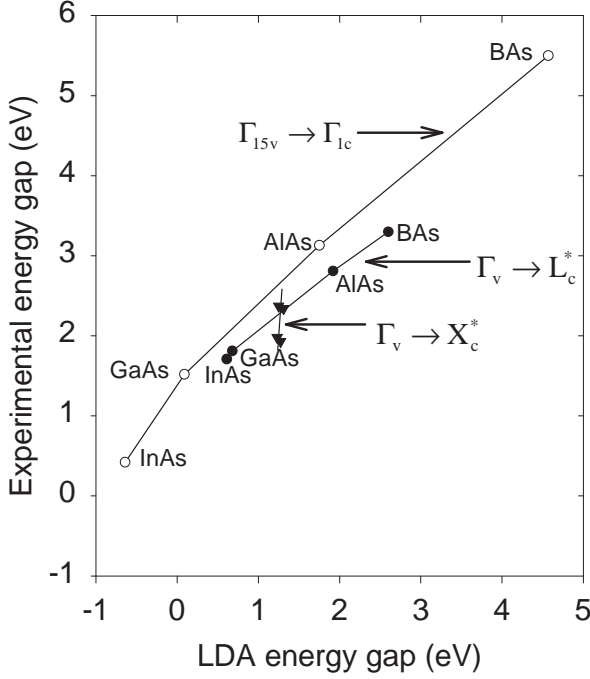


FIG. 7: Trends in the LDA vs. experimental band gaps of the III-As family. For the $\Gamma_{15v} \rightarrow \Gamma_{1c}$ and the $\Gamma_{15v} \rightarrow L_c$ gaps, the errors are nearly constant. The LDA errors are $\sim 1\text{--}1.5$ eV and $\sim 0.7\text{--}1.1$ eV for the $\Gamma_{15v} \rightarrow \Gamma_{1c}$ and the $\Gamma_{15v} \rightarrow L_c$ gaps, respectively.

to them. This effect is more pronounced for the $\Gamma_{1c} \rightarrow X_c$ difference because the lowest X conduction state has less s character than the lowest L conduction state.

D Charge density and ionicity trends in the III-As family

The valence charge density [upper four bands, d bands not included; Eq. (4)] in the (110) plane is shown for the four members of the III-As family in Fig. 9. We see that the charge densities of AlAs, GaAs, and InAs are drawn towards the anion and exhibit a “single hump” in the bond charge. (The relative shifts in the bond charge, d_{\max}/d_{bond} , are ~ 0.68 for AlAs and GaAs, and ~ 0.71 for InAs.) The relative shift of charge towards the anion (As) is due to the difference in electronegativity of the anion and the cation and reflects the partially ionic nature of the bond. In contrast, because of the almost entirely covalent nature of the bonding in the BAs system, in this system the charge density features a “double hump” bond similar to the bond charges in diamond C and Si.^{46,47} A similar analysis of the charge density of BAs was reported earlier by Wentzcovitch and Cohen.²⁰ We see that BAs is unique in the III-As family in that the bonding is very covalent. This is evidenced by the exceptionally strong hybridization of p states from the anion and cation (see

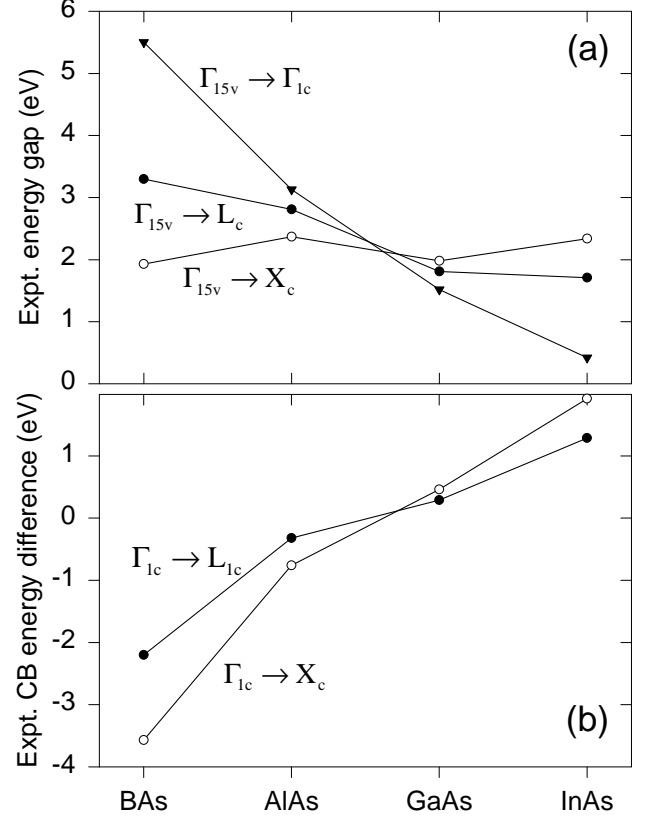


FIG. 8: Trends in the inter-valley energy separations of the III-As family. Note the crossing of the $\Gamma_{15v} \rightarrow X_c$ gaps and the $\Gamma_{15v} \rightarrow \Gamma_{1c}$ gaps between AlAs and GaAs. Thus, GaAs and InAs are direct gap materials whereas BAs and AlAs are indirect X gap materials.

Figs. 2, 5, and 6) and the significant bonding charge visible in the valence charge density which is similar to the bonding charge in diamond C and Si.

It is interesting to note that, in contrast to AlAs, GaAs, and InAs where charge is drawn towards the anion, the nearly symmetric bond charge distribution shown in the valence charge plot of BAs is not centered exactly around the bond center but is actually drawn slightly toward the *cation* B. (The distance between the bond center and the boron position is about 45% of the total bond length.) This would indicate that whatever small ionic component exists in BAs results not from charge transfer towards the *anion* but from charge transfer towards the *cation* B. Further evidence of an ionic component in BAs where the boron atom acts as the anion is shown in the valence charge difference plots [Eq. (5)] in Fig. 10. In AlAs, GaAs, and InAs, the maximum (marked as a cross) in $\Delta\rho_{\text{val}}$ occurs closer to the As anion than to the cation, consistent with the reported ionicities. However, in BAs, the maximum in $\Delta\rho_{\text{val}}$ occurs closer to the B atom. In addition, the positive region around the B atom in $\Delta\rho_{\text{val}}$, which does not occur for the other members of the III-As family, is further indication of a slight ionic component

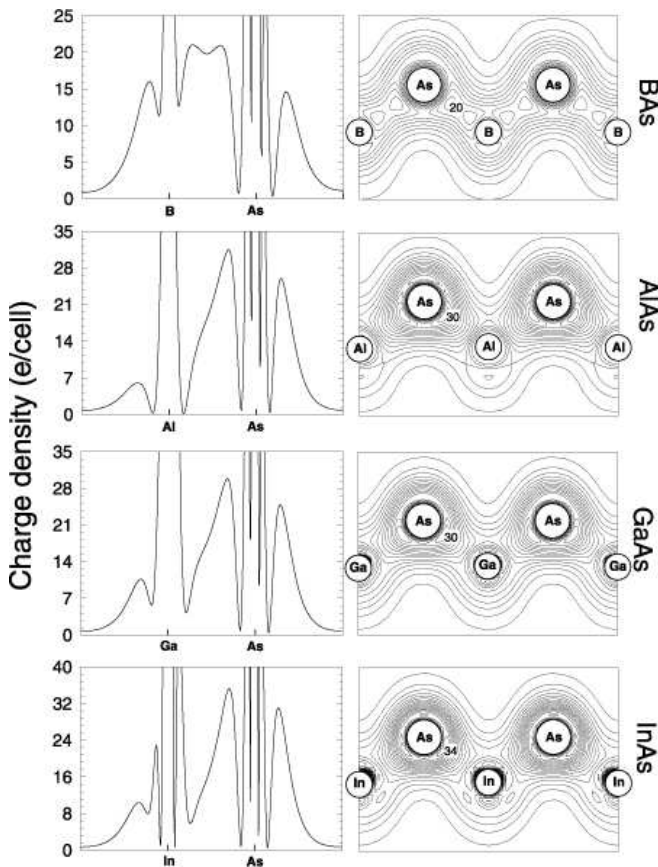


FIG. 9: Valence charge densities ρ_{val} [Eq. (4)] for the III-As family, excluding the cation and anion d states. The contour plots use the same scale as the corresponding line plots. The contour spacing is 2 e/cell. The range of the line plots is from one tetrahedral interstitial site, through the bond, and to the neighboring tetrahedral interstitial site. Note the striking asymmetry of the bonding charge for the three systems AlAs, GaAs, and InAs, while the bond charge in BAS reveals a covalent, double-hump feature similar to that found in diamond C, Si, or Ge.

in BAs where B plays the role of the *anion* rather than the cation. This reversal of the cation and anion roles in BAs (and in BP) is predicted by the Phillips scale of electronegativities⁴² and has been discussed previously by Wentzcovitch and Cohen.²⁰

IV. BAND OFFSETS: BAs/GaAs/AlAs

The offset $\Delta E_v(AX/BY)$ between the valence band maxima of two semiconductor compounds AX and BY forming a heterostructure is one of the most important parameters in interfacial structures deciding both transport and quantum confinement. The results for the natural (unstrained) band offsets [Eq. (6)] for BAs/GaAs and BAs/AlAs are plotted in Fig. 11. The *conduction* band

offsets shown in the figure are determined by adding the experimental gaps to the calculated valence band offsets. The natural band offset for AlAs/GaAs has been computed previously⁴⁸ and has been included here to contrast the offset behavior of “typical” heterojunctions and those of heterojunctions with BAs.

The ordering of the VBM of BAs in the III-As is somewhat surprising. Because the VBM decreases systematically in the order InAs \rightarrow GaAs \rightarrow AlAs [Fig. 11(b)], one might expect that the VBM of BAs would lie *below* AlAs, but in fact, the VBM of BAs is above AlAs, nearly as high as GaAs. The ordering of the VBMs for InAs, GaAs, and AlAs can be understood qualitatively using a tight-binding argument analogous to Eq. (11) for Γ_{15c} when a p - d term is added. The effects of this additional term are indicated schematically in Fig. 4b. The ordering of the VBMs is as follows:

InAs relative to GaAs: Two effects account for the slightly higher VBM of InAs relative to that of GaAs.⁴⁹ (i) InAs has a longer bond length than GaAs. This reduces E_{pp} of Eq. (11) and tends to drive the Γ_{15v} VBM up relative to GaAs. (ii) In tetrahedral symmetry, the cation d and anion p states share the same Γ_{15} symmetry and hence can interact through the potential matrix element $\langle \phi_{\text{cation}}^d | V | \phi_{\text{anion}}^p \rangle = E_{dp}$. The mostly anion p -like VBM is repelled upwards by the Ga/In d states by an amount $E_{dp}^2 / (\epsilon_p^{\text{anion}} - \epsilon_d^{\text{cation}})$. This p - d repulsion^{48,49} is slightly stronger in InAs where the cation $4d$ states are shallower and less localized than the Ga $3d$ state, as shown schematically in Fig. 4b.

GaAs relative to AlAs: The difference between the VBM of GaAs and AlAs can also be understood in terms of this p - d repulsion effect. In GaAs, the deep gallium d states couple to the arsenic p states, driving the VBM up, but in AlAs, there are no aluminum d states below the VBM. Instead, the interaction of the arsenic p states at the VBM and the *unoccupied* aluminum d states *above* the VBM drives the AlAs VBM *down*. Thus, p - d repulsion has the opposite effect on the VBM in GaAs and AlAs (Fig. 4b).

AlAs relative to BAs: Two effects increase the VBM of BAs relative to the VBM of AlAs. (i) Because the unoccupied d states in BAs lie very high in energy relative to the VBM, the p - d repulsion effect that drives the VBM down in AlAs is weaker in BAs. (ii) The more important effect is the unusual character of the VBM in BAs. In the rest of the III-As family, the character of the VBM is primarily anion p -like, but in BAs the bonding is much more covalent and the VBM comes from both the anion and the cation (Fig. 6). Since the cation p levels are higher in energy than the As p levels (Fig. 1), any admixture of cation p character pulls the VBM up. These two effects, lack of p - d repulsion and strong hybridization of the cation p character into the VBM, account for the high VBM of BAs relative to AlAs.

GaAs relative to BAs: While the VBM of BAs and GaAs both lie above that of AlAs for the reasons given above, the VBM of BAs lies only slightly below that of

GaAs despite the much smaller lattice constant ($\sim 17\%$ mismatch) and the lack of p - d repulsion. This is due to the unusual cation p hybridization into the VBM of BAs which raises the VBM by several tenths of an eV.

Finally, we note that the transitivity among the band offsets of BAs/AlAs/GaAs is similar to other compounds where the lattice mismatches are not as large. By transitivity we mean that the band offset $\Delta E_v(A/C)$ between two compounds A and C is well approximated as the sum of the band offsets between compounds A and B and between compounds B and C , i.e.,

$$\Delta E_v(\text{GaAs}/\text{BAs}) \cong \Delta E_v(\text{BAs}/\text{AlAs}) + \Delta E_v(\text{AlAs}/\text{GaAs}). \quad (13)$$

In this case, $\Delta E_v(\text{GaAs}/\text{BAs})$ calculated directly yields 0.19 eV but $\Delta E_v(\text{BAs}/\text{AlAs}) + \Delta E_v(\text{AlAs}/\text{GaAs})$ yields 0.12 eV, a non-transitivity difference of 0.07 eV.

V. BAs-GaAs ALLOYS

A Bond lengths and bond angles in the alloys

Interest in BAs-GaAs alloys centers around the hope that boron will modify the GaAs band gap similarly to nitrogen without the adverse effect⁵⁰ of introducing localized states that reduce carrier diffusion length. We know from the theory of III-V alloys^{29,51} that the optical properties are decided by both the atomic relaxation and by charge transfer. Thus, we first study the bond relaxation around a boron substitutional impurity.

The bond lengths and angles in the (110) plane of GaAs with $\sim 3\%$ boron substitution ($\text{B}_1\text{Ga}_{31}\text{As}_{32}$ supercell) are shown in Fig. 12. Bond lengths are shown as a percentage of the pure bulk GaAs bond length, except for the B-As bonds where the values indicate a percentage of the pure bulk BAs bond length. The numbers that lie between a triplet of atoms indicate the bond angle between the three atoms as a percentage of the ideal bond angle in the zinc-blende structure of 109.47° . The rectangle represents the supercell boundary. We note several observations:

(i) Bond angles near boron increase by up to 5% from their ideal value. This helps accommodate the Ga-As and B-As alloy bonds (hereafter R_{GaAs} and R_{BAs} , respectively) to keep the bond lengths close to their ideal values, R_{BAs}^0 and R_{GaAs}^0 in the pure binary compounds.

(ii) The B-As bond decreases from the GaAs value towards the BAs value and ends up only 4% higher than the value for pure BAs.

(iii) The average bond length relaxation parameter⁵²

$$\epsilon = [R_{\text{GaAs}}(x) - R_{\text{BAs}}(x)] / [R_{\text{GaAs}}^0 - R_{\text{BAs}}^0] \quad (14)$$

is 0.76. ($\epsilon = 0$ when there is no relaxation and 1 when the relaxation is full.) Thus, assuming R_{BAs} to be Vegard-like (as in VCA) overestimates the bond length by $\sim 13\%$.

We also modeled a 50%-50% random alloy using a 32-atom special quasirandom structure (SQS16 in Table II).³⁹ We found that the distribution of the bond lengths has the expected bimodal form for a random binary alloy,⁵³ and the B-As bonds are generally larger than the ideal B-As bond length while the Ga-As bond lengths are smaller than the ideal Ga-As bond length.

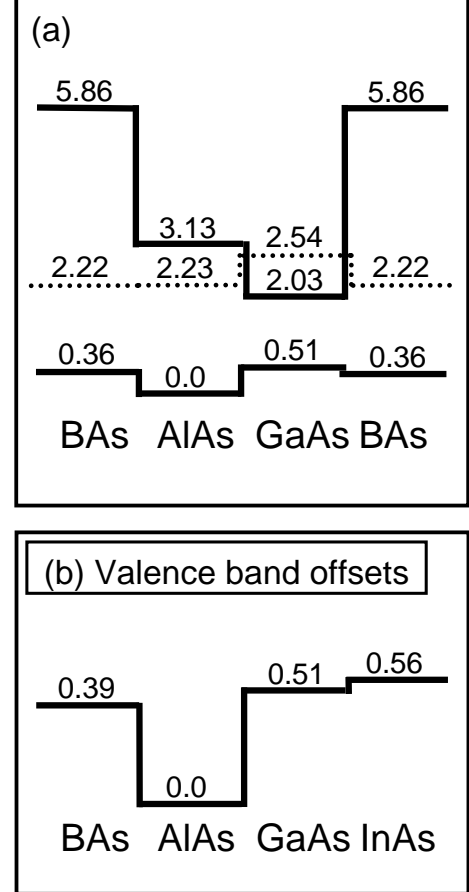


FIG. 11: Valence and conduction band offsets (in eV) for BAs/GaAs/AlAs and for the III-As family. The valence band offsets are calculated directly using Eq. (6). The conduction band offsets are obtained by adding the experimental band gap values to the valence band offsets. Part (a) shows the both the valence band and conduction band offsets for BAs/AlAs, AlAs/GaAs, and GaAs/BAs. Both the direct Γ_{15c} gap (solid line) and the X_{1c} gap (dotted line) are shown. The height of the BAs VBM was determined by averaging the valence band offsets of BAs with respect to AlAs and GaAs. Part (b) shows the valence band offsets in the III-As family. Surprisingly, the VBM of BAs is found to be above that of AlAs and not very far below that of GaAs.

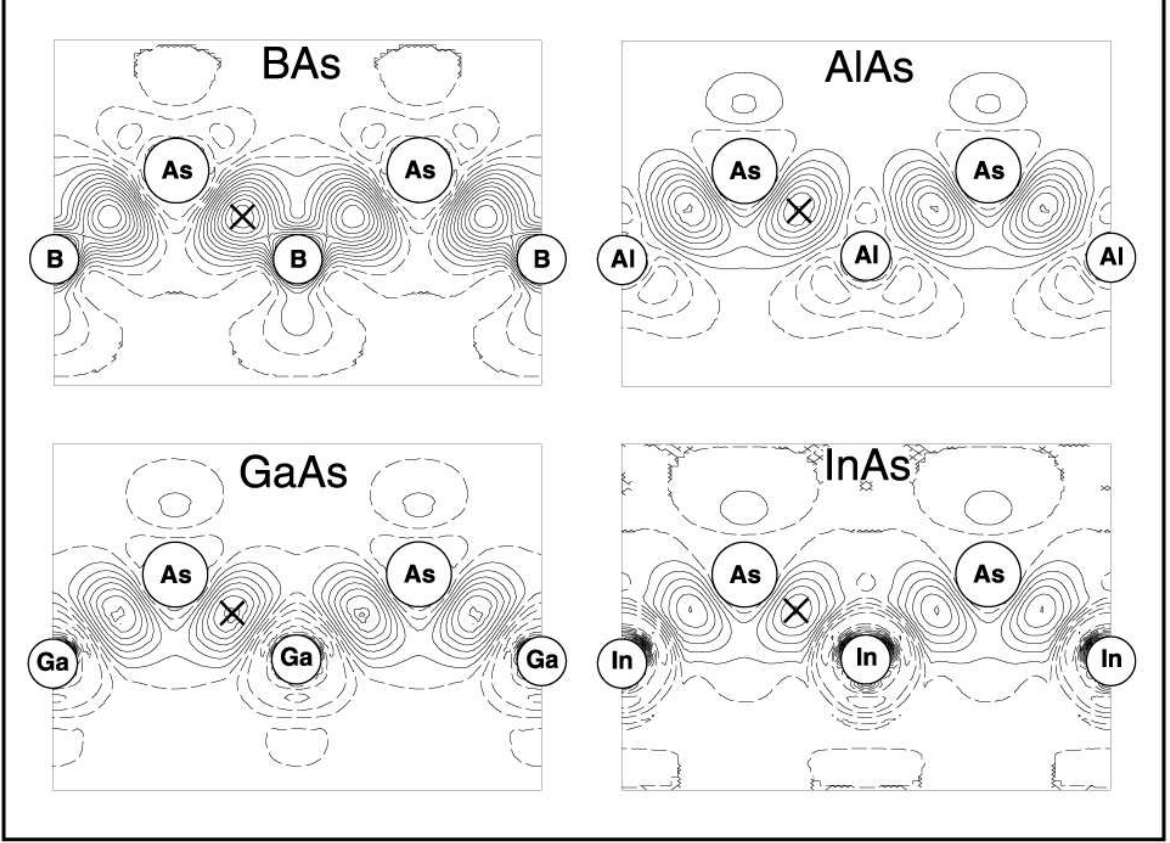


FIG. 10: Deformation density $\Delta\rho_{\text{val}}$ ($\rho_{\text{val}}^{\text{solid}} - \rho_{\text{val}}^{\text{atom}}$) plots for the III-As family in the (110) plane. Contours marked with dashed lines correspond to negative values of $\Delta\rho_{\text{val}}$. The units are $e/\text{\AA}^3$ and the contour spacing is 0.02. The maxima are marked by crosses. To determine $\Delta\rho_{\text{val}}$, the overlapping charge densities of free atoms are subtracted from the self-consistent charge density of the solid. The atomic configurations for the free atoms are $d^{10}s^2p^1$ and s^2p^3 for the cations and anions, respectively. The d bands of the cations, but not of the anions, are included in the valence bands.

B Bowing in the dilute alloy

Both measurements and calculations indicate that, for isoivalent semiconductor alloys, the deviation of the band gap, $\Delta E_g(x)$, from the average band gap, $\overline{E}_g(x)$, of the constituents is often well described by a quadratic term,^{29,51,54,55}

$$\Delta E_g(x) = bx(x - 1).$$

For typical semiconductor alloys, the bowing parameter b is normally less than 1 eV and is independent⁴⁵ of the concentration x . However, in $\text{GaAs}_{1-x}\text{N}_x$ alloys, where the lattice mismatch is large and the bond strength differences are significant, the bowing parameter is strongly composition dependent⁵⁶ and can be as large as 20 eV. Due to the large lattice mismatch of BAs and GaAs and the strong B-As bonds, one might expect that $\text{B}_x\text{Ga}_{1-x}\text{As}$ alloys would also show such large

and composition-dependent bowing. We calculated the $\Gamma_{15v} \rightarrow \Gamma_{1c}$ gaps in the experimentally-relevant composition range of 0–10%. The bowing was calculated using 64 atom supercells, as described in Sec. II. In this composition range, the direct $\Gamma_{15v} \rightarrow \Gamma_{1c}$ gap is the smallest gap. The bowing was calculated using the LDA $\Gamma_{15v} \rightarrow \Gamma_{1c}$ gaps of BAs, GaAs, (4.64 and 0.28 eV, respectively) and the LDA gaps at two alloy compositions, 3% and 6%. At the 3% composition, the bowing is $b = 3.4$ eV and at 6% the bowing is $b = 3.6$ eV. Thus, the band gap bowing is ~ 3.5 eV and relatively composition-independent in this composition range. A recent experimental study,¹⁸ estimated the bowing to be $b = 1.6 \pm 0.3$ or 2.3 ± 0.3 using *theoretical estimates* for the direct gap of cubic BAs of 3.56¹⁹ and 4.23.²² However, because of the LDA error in the band gaps (see Fig. 7), these estimated band gaps are too small, and thus, the bowing is underestimated. Because the LDA errors for the band gaps are

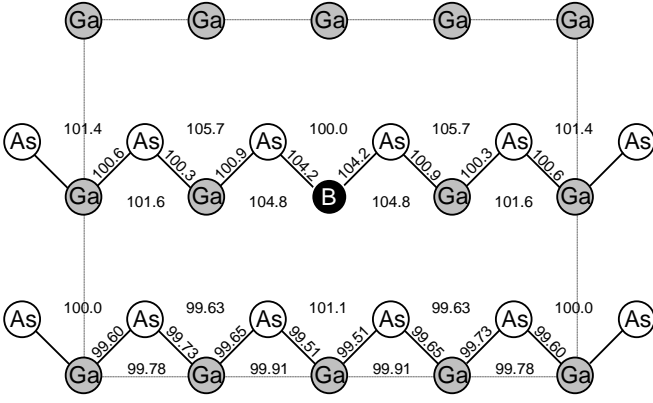


FIG. 12: Bond lengths and angles in $BGa_{31}As_{32}$ in the (110) plane. Bond lengths are shown as a percentage of the ideal GaAs bond length, except for the B–As bonds where the values indicate a percentage of the ideal BAAs bond length. The numbers that lie between a triplet of atoms indicate the bond angle between the three atoms as a percentage of the ideal bond angle in the zinc-blende structure of 109.47° . The rectangle represents the supercell boundary.

approximately constant for the III–As series, the bowing can be reliably calculated if *all* the points (E_A , E_B , and $E_{A_{1-x}B_x}$) are taken consistently from LDA calculations (as we did) because only the relative values are important. For computing the band gap bowing from experimental alloy data, the *GW* estimate of the BAAs direct band gap (5.5 eV),²⁴ which corrects LDA errors, is a more appropriate value to use to calculate the bowing. Using the experimental alloy data from Ref. 18, the *GW*-estimated band gap for BAAs (5.5 eV), and the experimental value of 1.42 eV for GaAs, Geisz estimates⁵⁷ the revised bowing parameter to be ~ 3.5 eV in excellent agreement with the theoretical prediction.

The bowing of $B_xGa_{1-x}As$ is much smaller than the bowing for $GaAs_{1-x}N_x$ alloys in the same range. Accordingly, we predict that addition of boron to GaAs will *raise* the gap. For example, the predicted gaps for 2%, 3%, 5% or 10% concentrations of boron, the band gaps would be 1.43, 1.44, 1.46, and 1.51 eV, respectively. Thus, the addition of boron to GaAs will not lead to a 1 eV gap alloy as seen with nitrogen addition. We also find that the bowing is composition independent. This implies that the effects of boron on the band gap in GaAs are much less pronounced than those of nitrogen. This is not completely unexpected, however, as it has been previously observed that the bowing is smaller in mixed cation systems than in mixed anion systems.²⁹

We have also calculated the band gap of the $BGa_{31}As_{32}$ CuPt-ordered compound finding that it is 0.12 eV below the 50%–50% random alloy modeled via the SQS16.

C Enthalpy of mixing and stability of superlattices

Table V gives the formation enthalpies [Eq. (9)] for (001) *ordered superlattices* of BAAs/GaAs and the mixing enthalpies of $B_xGa_{1-x}As$ *random alloys*. The formation energy of ordered superlattices of orientation \hat{G} and period n is

$$\Delta H(n, \hat{G}) = E(A_n B_n; \hat{G}) - \frac{1}{2}(E_A + E_B) \quad (15)$$

can be separated into two contributions:⁵⁸ (i) The constituent strain energy, i.e. the energy of the infinite period superlattice. This is the strain energy associated with deforming pure A and pure B into the in-plane lattice constant \bar{a} of the superlattice, and relaxing them in the direction \hat{G} . (ii) The interfacial energy, i.e., the difference between $\Delta H(n, \hat{G})$ and the constituent strain energy, is defined by

$$\Delta H(n, \hat{G}) = \frac{2I(n, \hat{G})}{n} + \Delta E_{CS}(\bar{a}, \hat{G}). \quad (16)$$

We calculated $\Delta E_{CS}(\bar{a}, \hat{G})$ for BAAs and GaAs, deformed to the average lattice constant \bar{a} along $\hat{G} = (001)$. This gave 148 meV/atom. From $\Delta H(n, \hat{G} = 001)$ of Table V and ΔE_{CS} we calculated the interfacial energy I for $n = 1, 2$, and 4. We found $I = 19, 23$, and 26 meV, respectively. While a larger superlattice period n would be required to determine the converged value of I , we see that the BAAs-GaAs interface is *repulsive*. This is why $\Delta H(n, \hat{G})$ of Table V *decreases* with n : larger n reduces the *proportional* effect of the interfacial repulsion.

So far we dealt with (001) superlattices. The monolayer $(BAAs)_1/(GaAs)_1$ (111) is particularly interesting since in other III–V alloys (e.g., GaInP₂) it appears as a spontaneously ordered structure during alloying.⁵⁹ We find a very high $\Delta H(CuPt)$ of 108 eV/atom, suggesting thermodynamic instability.

For the random alloys in Table V, all of the excess enthalpies are positive. We compare the mixing enthalpies as obtained by the LDA (which includes both size-mismatched-induced strain effects and charge-transfer “chemical” effects) and the valence force field (VFF) method (which includes only strain effects). The trends and magnitudes are similar, showing that the strain effects dominate ΔH . In Fig. 13 we compare the VFF-calculated mixing enthalpy of nitrogen in GaAs and contrast it with that of boron in GaAs, showing that the mixing enthalpy of $GaAs_{1-x}N_x$ alloys is much higher than for $B_xGa_{1-x}As$ alloys. These results indicate that it may be easier to alloy boron with GaAs. This implies that the range of *bulk* $B_xGa_{1-x}As$ alloy compositions could be substantially larger than for the nitride alloy $GaAs_{1-x}N_x$. In *epitaxial* growth experiments, the alloy solubility can dramatically exceed that in *bulk* experiments for reasons explained in Ref. 60.

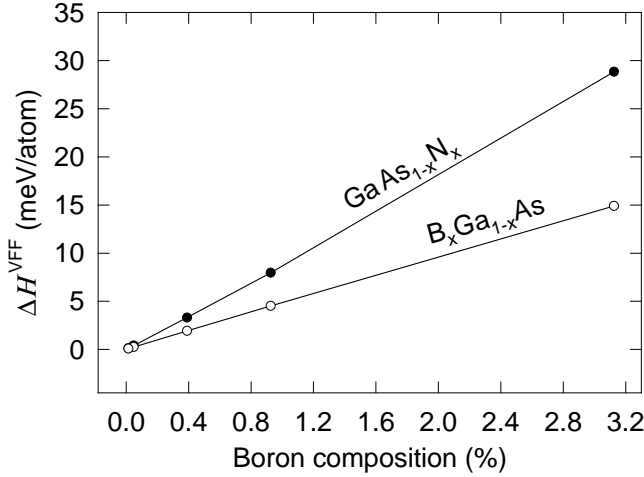


FIG. 13: Calculated VFF mixing enthalpies for dilute $\text{GaAs}_{1-x}\text{N}_x$ alloys and dilute $\text{B}_x\text{Ga}_{1-x}\text{As}$ alloys. The mixing enthalpy is substantially smaller for boron alloys.

D Quasi-localized electronic states

We find that the incorporation of boron into the GaAs host material has little effect on the state at the VBM but that the lower conduction band states are strongly perturbed. The square of the wavefunctions for the VBM and the lowest two conduction band states for isolated boron in GaAs are shown in the left hand side of Fig. 14. The first column shows the states for an isolated boron atom in the center of a supercell of GaAs. The VBM is completely delocalized and looks very much like the VBM state of pure GaAs except for a region near boron impurity where the wavefunction is extended towards the boron atom. This distortion is precisely what one would expect based on the strong coupling of boron p and arsenic p states at the VBM in BAs, as discussed in Secs. III B and III D. In contrast to the VBM, the CBM state shows a significant localization around the boron atom. The CBM shows *long range* delocalization, but the majority of the wavefunction is concentrated near the boron atom. For the second lowest conduction band state (CBM+1), the situation is similar except the wavefunction is concentrated around a small number of gallium atoms as well. The dual character of the conduction band states (extended at long range but concentrated around the boron atoms in the short range) indicates that the states are *resonant* in the conduction band and are not localized states *inside the gap*. The conduction band states could be considered as boron-perturbed bulk GaAs conduction band states.

The second column of Fig. 14 shows the same states (VBM, CBM, CBM+1) for a fourth neighbor *pair* of boron atoms inside a supercell of GaAs. A statistically random distribution of boron atoms would result, among others, in pairs. In the case of $\text{GaAs}_{1-x}\text{N}_x$ alloys, the

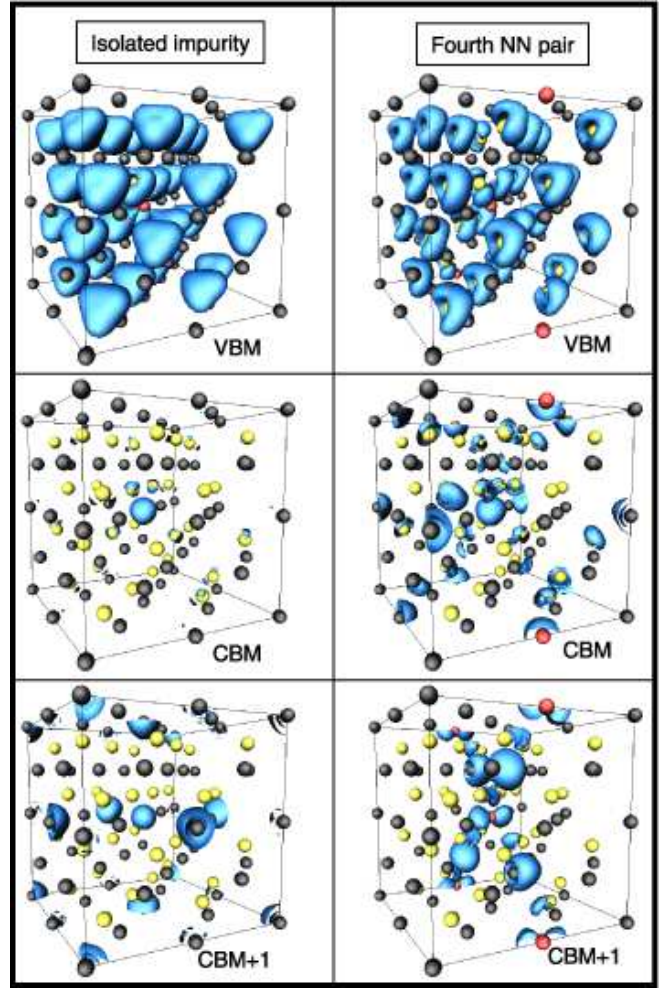


FIG. 14: (color) Isosurfaces of the wavefunction squared for a single impurity and for a fourth nearest neighbor pair. Boron atoms are red, gallium black, and arsenic yellow. The isosurface value (blue) is $0.01 \text{ e}/\text{\AA}^3$. In both cases, the VBM states are completely delocalized and are primarily As-derived. The lower conduction band states are strongly concentrated around the boron atoms.

presence of nitrogen pairs can result in localized impurity states inside the gap.⁶¹ Calculations were performed for the five symmetrically-unique pair arrangements in the 64 atom supercell as described in Table III. Qualitative features of wavefunction localization were the same for all of the pairs, and only the most representative case, the fourth nearest neighbor pair, is shown in the figure. The features of the pair states are similar to those of the isolated impurity discussed above—that is, the VBM is mainly an As-derived, delocalized state while the lower CB states are concentrated around the boron atoms. Again, there is some effect on the wavefunction very near the boron atom. The CBM state is concentrated around the boron atom in the middle of the cell and around the boron and gallium atoms on the cell edges. The next low-

est conduction band state shows similar features and the wavefunction is restricted primarily to the (200) plane of the cell.

The short-range “localization” effects of boron incorporation into GaAs appear to be similar to those seen in $\text{GaAs}_{1-x}\text{N}_x$ alloys, resulting mainly in “dual character” conduction band states that are still extended at long range but are localized around the boron atoms. However, it appears that the perturbation of boron on the near-gap states of GaAs is gentler than that of nitrogen as none of the pairs cause states inside the gap. This is another instance (as with band gap bowing and band offsets) where boron is less “intrusive” than its first-row cousin, nitrogen.

VI. CONCLUSIONS

This paper explored the effects of alloying a conventional III–V compound, GaAs, with boron. Very little has been known, experimentally or theoretically about boride III–V semiconductor alloys, but boride semiconductor alloys are generating renewed interest now that epitaxial techniques have made it somewhat easier to fabricate them. In order to understand the fundamentals of this new class of possible alloys. We have studied zincblende BAs and its alloy with GaAs.

For BAs we find: (i) The bonding in BAs is much more covalent than in the rest of the III–As family or other III–Vs. This is due to the similar electronegativities of boron and arsenic. (ii) Consequently, BAs has a nearly symmetric, “double-hump” bond charge density, similar to silicon. The small asymmetry that does exist in the bonding charge density actually favors *boron*. That is, charge is drawn toward the boron atom. In this sense, boron behave more like the *anion* than the *cation* in BAs. (iii) The band structure of BAs is more reminiscent of silicon than most other III–V compounds. This is a consequence of (1) the small repulsion between bonding and antibonding *p* states and (2) the large repulsion of the arsenic and boron *s* states. (iv) The LDA errors in the band gaps are approximately constant in the III–As series BAs, AlAs, GaAs, and InAs. (v) The band offsets of BAs/GaAs and BAs/AlAs are unexpected. The VBM of BAs is 0.39 eV higher than AlAs and only 0.19 eV below GaAs. The main reason for this is the strong hybridization of both the cation and anion states at the VBM.

For the $\text{B}_x\text{Ga}_{1-x}\text{As}$ alloys, we find that: (i) The bond angles are highly distorted near the boron sites. This accommodates the Ga–As and B–As bonds to stay close to their ideal bulk values. As a result, the bond length distribution in a random alloy exhibits the typical bimodal behavior where each mode is near the individual ideal bulk values. (ii) The bowing parameter of $\text{B}_x\text{Ga}_{1-x}\text{As}$ for low concentrations of boron is 3.5 eV, much smaller than for $\text{GaAs}_{1-x}\text{N}_x$ alloys in the same composition

range. Consequently, unlike GaN, alloying GaAs with small amounts (< 10%) of BAs *increases* the gap. (iii) The enthalpies of mixing indicate that the bulk solubility of boron in GaAs may be significantly higher than nitrogen in GaAs, possibly increasing the composition range over which boride alloys may be formed. (iv) The wavefunction of the VBM is completely delocalized and retains the character of pure GaAs. The lower conduction band states exhibit a “semi-localized” behavior—i.e. the states are strongly concentrated around the boron atoms, but far away they are extended states.

In summary, the behavior of $\text{B}_x\text{Ga}_{1-x}\text{As}$ alloys is qualitatively different from $\text{GaAs}_{1-x}\text{N}_x$ alloys. The perturbation of boron in GaAs is much “gentler” on most features of the electronic structure of GaAs than is nitrogen. If the same behavior is manifest for other boride III–V alloys, boron offers a new class of III–V alloys to be explored for novel behavior and possible device applications. Boron may also play an important role in alloys where it could be used as a relatively benign component which is added to lattice match the alloy to a given substrate.

VII. ACKNOWLEDGEMENTS

Supported by DOE-SC-BES-DMS under contract No. DE-AC36-99-GO10337. We gratefully acknowledge S.-H. Wei for many helpful discussions regarding the LAPW method and a critical reading of the manuscript, and J. F. Geisz for useful discussions regarding the experimental data and techniques as well as a critical reading of the manuscript.

REFERENCES

- ¹ R. Addinall, R. C. Newman, Y. Okada, and F. Orito, *Semicond. Sci. Technol.* **7**, 1306 (1992).
- ² R. C. Newman, “Local Vibrational Mode Spectroscopy of Defects in III/V Compounds,” in *Semiconductors and Semimetals* (Academic Press, 1993), Vol. 38.
- ³ J. Maguire, R. C. Newman, I. Grant, D. Rumsby, and R. M. Ware, *J. Phys. D: Appl. Phys.* **18**, 2029 (1985).
- ⁴ J. Woodhead, R. C. Newman, I. Grant, D. Rumsby, and R. M. Ware, *J. Phys. C: Solid State Phys.* **16**, 5523 (1983).
- ⁵ G. A. Gledhill, R. C. Newman, and J. Woodhead, *J. Phys. C: Solid State Phys.* **17**, L301 (1984).
- ⁶ S. B. Zhang and D. J. Chadi, *Phys. Rev. Lett.* **64**, 1789 (1990).
- ⁷ M. A. Tischler, P. M. Mooney, B. D. Parker, F. Cardone, and M. S. Goorsky, *J. Appl. Phys.* **71**, 984 (1992).
- ⁸ W. E. Hoke, P. J. Lemonias, D. G. Weir, and H. T. Hendricks, *J. Vac. Sci. Technol. B* **11**, 902 (1992); S.

- K. Brierley, H. T. Hendricks, W. E. Hoke, P. J. Lemoias, D. G. Weir, *Appl. Phys. Lett.* **63** 812 (1993).
- ⁹ L. B. Ta, H. M. Hobgood, and R. N. Thomas, *Appl. Phys. Lett.* **41**, 1091 (1982).
- ¹⁰ S. M. Ku, *J. Electrochem. Soc.* **113**, 813 (1966).
- ¹¹ S. Sakai, Y. Ueta, and Y. Terauchi, *Jpn. J. Appl. Phys.* **32**, 4413 (1993).
- ¹² V. G. Vorob'ev, Z. S. Medvedeva, and V. V. Sobolev, *Izv. Akad. Nauk SSSR, Neorg. Mater. [Inorg. Mater. (USSR)]* **3**, 959 (1967).
- ¹³ T. L. Chu and A. E. Hyslop, *J. Appl. Phys.* **43**, 276 (1972); *J. Electrochem. Soc.: Solid-State Sci. Tech.* **121**, 412 (1974).
- ¹⁴ A. J. Perri, S. LaPlaca, and B. Post, *Acta Cryst.* **11**, 310 (1958).
- ¹⁵ F. V. Williams and R. A. Ruehrwein, *J. Am. Chem.* **82** 1330 (1960).
- ¹⁶ H. M. Manasevit, W. B. Hewitt, A. J. Nelson, and A. R. Mason, *J. Electrochem. Soc.* **136**, 3070 (1989).
- ¹⁷ M. L. Timmons, Final Technical Report for *Very High Efficiency Solar Cells*, Department of Defense, Office of Contracts, Contract #NRO-95-C-3001, 1998.
- ¹⁸ J. F. Geisz, D. J. Friedman, J. M. Olson, Sarah R. Kurtz, R. C. Reedy, A. B. Swartzlander, B. M. Keyes, and A. G. Norman, *Appl. Phys. Lett.* **76** 1443 (2000).
- ¹⁹ D. J. Stukel, *Phys. Rev. B* **1**, 3458 (1970).
- ²⁰ R. M. Wentzcovitch and M. L. Cohen, *J. Phys. C: Solid State Phys.* **19**, 6791 (1986).
- ²¹ R. M. Wentzcovitch, M. L. Cohen, and P. K. Lam, *Phys. Rev. B* **36**, 6058 (1987).
- ²² C. Prasad and M. Sahay, *Phys. Stat. Sol. (b)*, **154**, 201 (1989).
- ²³ M. Ferhat, A. Zaoui, M. Certier, H. Aourag, *Physica B* **252**, 229 (1998).
- ²⁴ M. P. Surh, S. G. Louie and M. L. Cohen, *Phys. Rev. B* **43**, 9126 (1991).
- ²⁵ F. Benkabou, C Chikr.z, H. Aourag, P. J. Becker and M. Certier, *Physics Letters A* **252**, 71 (1999).
- ²⁶ B. Bouhafs, H. Aourag, M. Ferhat, and M. Certier, *J. Phys.: Condens. Matter* **11** 5781 (1999).
- ²⁷ T. Mattila, S.-H. Wei, and A. Zunger, *Phys. Rev. B* **60**, R11 245 (1999).
- ²⁸ L. Bellaiche, T. Mattila, S.-H. Wei, and A. Zunger, *Phys. Rev. B* **74**, 1842 (1999).
- ²⁹ S.-H. Wei and A. Zunger, *Phys. Rev. B*, **43**, 1662 (1991); *ibid.*, *J. Appl. Phys.* **78**, 3846 (1995); *ibid.*, *Phys. Rev. Lett.* **76**, 664 (1996).
- ³⁰ P. Hohenberg and W. Kohn, *Phys. Rev. B* **136**, B864 (1964); W. Kohn and L. J. Sham, *ibid.* **140**, A1133 (1965).
- ³¹ S.-H. Wei and H. Krakauer, *Phys. Rev. Lett.* **55**, 1200 (1985), and references therein; D. J. Singh, *Planewaves, Pseudopotential and the LAPW Method* (Kluwer Academic Publishers, Boston, 1994), and references therein.
- ³² D. J. Singh, *Phys. Rev. B* **43**, 6388 (1991).
- ³³ P. Blaha, K. Schwarz, and J. Luitz, WIEN97, Vienna University of Technology, Vienna, 1997; Updated version of P. Blaha, K. Schwarz, P. Sorantin, and S. B. Trickey, *Comput. Phys. Commun.* **59**, 399 (1990).
- ³⁴ J. P. Perdew and Y. Wang, *Phys. Rev. B* **45**, 13244 (1992).
- ³⁵ H. J. Monkhorst and J. D. Pack, *Phys. Rev. B* **13** 5188 (1976).
- ³⁶ S. Froyen, *Phys. Rev. B* **39**, 3168 (1989).
- ³⁷ Tetrahedral radii are (in angstroms): boron 0.853, aluminum 1.230, gallium and arsenic 1.225, and indium 1.405. J. C. Phillips, *Bonds and Bands in Semiconductors* (Academic Press, New York and London, 1973) p. 22.
- ³⁸ S. P. Kowalczyk, J. T. Cheung, E. A. Kraut, and R. W. Grant, *Phys. Rev. Lett.* **56**, 1605 (1986); T. M. Duc, C. Hsu, and J. P. Faurie, *ibid.* **58**, 1127 (1987).
- ³⁹ A. Zunger, S.-H. Wei, L. G. Ferreira, and J. E. Bernard, *Phys. Rev. Lett.* **65**, 353 (1990); S.-H. Wei, L. G. Ferreira, J. E. Bernard, and A. Zunger, *Phys. Rev. B* **42**, 9622 (1990).
- ⁴⁰ P. N. Keating, *Phys. Rev.* **145**, 637 (1966); R. M. Martin, *Phys. Rev. B* **1**, 4005 (1970).
- ⁴¹ A. J. Williamson, L. W. Wang, and A. Zunger, condmat/0003055, preprint.
- ⁴² According to Phillip's scale of electronegativity (Ref. 37, pg. 54), boron has a slightly *higher* electronegativity than arsenic. According to Pauling's scale of electronegativities, the electronegativities of boron and arsenic are the same.
- ⁴³ W. A. Harrison, *Electronic Structure and the Properties of Solids*, (W. H. Freeman and Company, San Francisco, 1980).
- ⁴⁴ S.-H. Wei and A. Zunger, *Phys. Rev. B* **57**, 8983 (1998).
- ⁴⁵ *Semiconductors. Physics of Group IV and III-V compounds*, edited by O. Madelung, M. Shulz, and H. Weiss, Landolt-Börnstein, New Series, Group III, vol. 17, pt. A (Springer-Verlag, Berlin, 1982); *Intrinsic Properties of Group IV Elements and III-V, II-VI, and I-VII Compounds*, edited by O. Madelung, M. Shulz, and H. Weiss, Landolt-Börnstein, New Series, Group III, vol. 22, pt. A (Springer, Berlin, 1987).
- ⁴⁶ C. S. Wang and B. M. Klein, *Phys. Rev. B* **24**, 3393 (1981)
- ⁴⁷ Z. W. Lu and A. Zunger, *Phys. Rev. B* **47**, 9385 (1993).
- ⁴⁸ S.-H. Wei and A. Zunger, *Appl. Phys. Lett.* **72**, 2011 (1998).
- ⁴⁹ S.-H. Wei and A. Zunger, *Phys. Rev. Lett.* **59**, 144 (1987).
- ⁵⁰ J. F. Geisz, D. J. Friedman, Sarah R. Kurtz, and B. M. Keyes, *J. Cryst. Growth* **195**, 401 (1998).
- ⁵¹ R. Magri, S. Froyen, and A. Zunger, *Phys. Rev. B* **44**, 7947 (1991).
- ⁵² J. L. Martins and A. Zunger, *Phys. Rev. B* **30**, 6218 (1984).
- ⁵³ J. C. Mikkelsen and J. B. Boyce, *Phys. Rev. Lett.* **49**, 1412 (1982); *Phys. Rev. B* **28**, 7130 (1983); J. B. Boyce and J. C. Mikkelsen, *Phys. Rev. B* **31**, 6903 (1985).

- ⁵⁴ *Landolt-Bornstein: Numerical Data and Functional Relationships in Science and Technology*, edited by O. Madelung, M. Schulz, and H. Weiss (Springer-Verlag, Berlin, 1982), Vol. 17a.
- ⁵⁵ J. E. Bernard and A. Zunger, Phys. Rev. B **36**, 3199 (1987)
- ⁵⁶ L. Bellaiche, S.-H. Wei, and A. Zunger, Phys. Rev. B **56**, 10233 (1997).
- ⁵⁷ J. F. Geisz, private communication.
- ⁵⁸ R. G. Dandrea, J. E. Bernard, S.-H. Wei, and A. Zunger, Phys. Rev. Lett. **64**, 36 (1990).
- ⁵⁹ A. Zunger and S. Mahajan, "Atomic Ordering and Phase Separation in III-V Alloys," in *Handbook of Semiconductors*, Vol. 3, second edition, Elsevier, Amsterdam, p. 1399-1513 (1994).
- ⁶⁰ S. B. Zhang and Alex Zunger, Appl. Phys. Lett. **71**, 677 (1997).
- ⁶¹ X. Liu, M.-E. Pistol, L. Samuelson, S. Schwetlick, and W. Seifert, Appl. Phys. Lett. **56**, 1451 (1990).